Decomposing the collision operator in the lattice Boltzmann method

Julius Weinmiller,[1,2,*] Benjamin Kellers,[1,2] Martin P. Lautenschlaeger,[3] Arnulf Latz,[1,2,4] and Timo Danner[1,2,†]

[1]*Institute of Engineering Thermodynamics, German Aerospace Center (DLR), Ulm, Germany*

[2]*Helmholtz Institute Ulm for Electrochemical Energy Storage (HIU), Ulm, Germany*

[3]*SDU Mechatronics, Department of Mechanical and Electrical Engineering, University of Southern Denmark (SDU), Sønderborg, Denmark*

[4]*Institute of Electrochemistry, Ulm University, Ulm, Germany*

(Received 6 March 2024; accepted 13 March 2026; published 7 April 2026)

In transport theory, physical phenomena are well described using the Boltzmann equation, which is efficiently simulated and discretized with the lattice Boltzmann method. The collision step defines the microscopic molecules behavior, and thus the simulated physical phenomena. For complex phenomena, the collision step becomes complex as well. In this paper, we propose a framework to systematically decompose the collision step into individual collision rules. Each collision rule is easier to understand, and thus a faster understanding of the whole is achieved. By inverting the process, i.e., composing multiple collision rules together, one can create collision steps that can better describe the underlying complex phenomena. This framework's applications are manyfold, from both a theoretical and an application standpoint. Shown here is the decomposition of the Robin boundary condition into the Dirichlet and Neumann boundary conditions, extending it to a partial Robin boundary condition and semipermeable reactive membranes.

DOI: 10.1103/b1jh-dm6d

I. INTRODUCTION

Complex physical phenomena are a combination of multiple processes that collectively create intricate behavior. The effects of these processes are often convoluted and cannot be easily separated. However, computational approaches are popular to study such phenomena. A prerequisite for accurate simulations is that the model's abstraction and numerical scheme captures this complexity.

The lattice Boltzmann method (LBM) is a powerful computational technique for simulating transport phenomena and related processes, known for its inherent simplicity and versatility [1,2]. It represents microscopic particles using a discrete-velocity distribution function—the so-called population—in a discretized phase space, using lattices, for velocity and space, respectively. The macroscopic properties and behavior emerge through the collision and streaming of populations. In LBM, simple and local collision steps can already capture fluid flow in complex geometries very well, which is one aspect making the method so popular. However, only a single collision step can be applied to a grid location. This collision step needs to describe the underlying processes. Using only simple collisions may limit the applicability of LBM, while complex collisions are difficult to comprehend and implement into simulations.

Therefore, an easier development of more complicated collision steps for complex phenomena is key to mitigate these limitations. A promising strategy is to combine simple and well-known collision rules to create advanced and interpretable collision steps, which are able to describe complex physical phenomena. In our framework we refer to these schemes as composite collisions.

In literature, composite collisions, although not naming it as such, have been described for several phenomena. Approaches often have in common that relevant length and timescales of constitutive processes are not resolved. Most prominently, this approach has been used in the context of unresolved solid-fluid interaction, often called gray LBM or partial bounceback methods [3–10] used to simulate single- and multiphase flow within unresolved porous media [11–20]. Other applications are material dissolution [21–24], and (sharp) interface handling for both fluid-solid and solid-solid [4,25–32].

In our previous work [33] on reactive boundary conditions [33–37], we could demonstrate how careful analysis of existing boundary schemes can shed new insight into their behavior. Therefore, while this is not a new concept, a framework is missing for the analysis of existing and the development of new collision steps. This is an essential step to relate complex macroscopic behavior to microscopic collisions.

In the following, we present a versatile composite collision framework (CCF) for LBM. This framework provides a systematic approach to develop collision steps for complex physical phenomena by combining various simple collision rules. We first present the CCF in Sec. II A. Collision rules

*Contact author: julius.weinmiller@dlr.de

†Contact author: timo.danner@dlr.de

used in this paper are described in Sec. II B, and we present a discussion on forces in Sec. II C. Finally, in Sec. III, we apply the framework to our use cases, reinterpreting the reactive boundary condition and presenting two new collision steps for partial reactive boundary conditions and reactive membranes.

II. METHODOLOGY

The LBM solves the discrete form of the continuous Boltzmann equation,

$$\frac{\partial \tilde{f}}{\partial t} + \xi_\alpha \frac{\partial \tilde{f}}{\partial x_\alpha} + \frac{K_\alpha}{\rho}\frac{\partial \tilde{f}}{\partial \xi_\alpha} = \Omega[\tilde{f}] + Q. \tag{1}$$

The $\tilde{f}$ is the density distribution function, Ω is the collision operator, $\boldsymbol{K}$ is the applied force density, Q is a mass source, and $\boldsymbol{\xi}$ is the continuous microscopic velocity. The zeroth and first moments in $\boldsymbol{\xi}$ of $\tilde{f}$ are the density ρ and density momentum $\rho\mathbf{u}$. Additionally, $\boldsymbol{x}$ and t denoting space and time. When using index notation, the Greek subscripts indicate space.

A. Composite collision framework

The CCF is based on the idea of decomposition of the collision step. We can express any collision step as a sum of component collision rules Ω^n, each weighted with a component fraction η^n,

$$\Omega[\tilde{f}] = \sum_n \eta^n \Omega^n[\tilde{f}], \quad \sum_n \eta^n = 1. \tag{2}$$

The aim is to choose component collision rules Ω^n which are simpler and better understood. This improves interpretation of Ω and the total behavior can be understood by the sum of its parts.

In LBM, the Boltzmann equation with decomposed collision step Eqs. (1) and (2) is discretized to

$$f_i(\boldsymbol{x} + \mathbf{c}_i\Delta t, t + \Delta t) - f_i(\boldsymbol{x}, t) = \sum_n (\eta^n(\boldsymbol{x}, t)\Omega^n[f_i(\boldsymbol{x}, t)] + S_i^n(\boldsymbol{x}, t))\Delta t. \tag{3}$$

Here Δt is the time step. The roman subscripts, e.g., i, is used as the index for velocity space. As is usual in LBM, f_i are a redefined version of $\tilde{f}$ which ensures second-order accurate time discretization. Then $\mathbf{c}_i$ is the discrete microscopic velocity along the ith lattice direction. The S_i^n are the mass and momentum source terms emerging from Q and $\boldsymbol{K}$. The shorthand notations $f_i = f_i(\boldsymbol{x}, t)$ and $\eta^n = \eta^n(\boldsymbol{x}, t)$ are used throughout this paper. Computationally, this discretized form is often split into a collision and subsequent streaming step.

When $\Omega^n[f_i]$ is linear in f_i, as are most collision steps, then η^n can be pulled into the collision rule to form

$$\eta^n\Omega^n[f_i] \Longleftrightarrow \Omega^n\big[f_i^n\big], \quad f_i^n := \eta^n f_i. \tag{4}$$

The total population is the sum of the component population $f_i = \sum_n f_i^n$.

This notation suggests the interpretation of f_i^n as component populations. Each individual component population behavior and moments can be analyzed separately. Below are the component density ρ^n and momentum $(\rho\mathbf{u})^n$, including the "half-source" correction emerging from the second-order time discretization,

$$\rho^n := \sum_i f_i^n + \frac{\Delta t}{2}\sum_i \big(\Omega^n\big[f_i^n\big] + S_i^n\big) = \sum_i f_i^n + \frac{1}{2}\Delta\rho^n, \tag{5}$$

$$(\rho\mathbf{u})^n := \sum_i f_i^n\mathbf{c}_i + \frac{\Delta t}{2}\sum_i \big(\Omega^n\big[f_i^n\big] + S_i^n\big)\mathbf{c}_i, = \sum_i f_i^n\mathbf{c}_i + \frac{1}{2}\Delta(\rho\mathbf{u})^n. \tag{6}$$

The density, ρ, and momentum, $\rho\mathbf{u}$, of the full Boltzmann equation [cf. Eq. (1)] are the sum of the n-specific components via

$$\rho = \sum_n \rho^n = \sum_i f_i + \frac{1}{2}\sum_n \Delta\rho^n, \tag{7}$$

$$\rho\mathbf{u} = \sum_n (\rho\mathbf{u})^n = \sum_i f_i\mathbf{c}_i + \frac{1}{2}\sum_n \Delta(\rho\mathbf{u})^n. \tag{8}$$

So far, neither Ω^n nor S_i^n have been defined to keep the formulation as general as possible. They need to be chosen such that together they match the physical phenomena studied. As a trivial example, fluid flow can be recovered with a single collision rule $n = \text{BGK}$ and $\eta^{\text{BGK}} = 1$. In Appendix A, we detail a more involved analytical example for Darcy flow, and how to derive η^n. Alternatively to analytical investigations, one can use toy problems to match η^n to relevant physical characteristics, experimental results or benchmarks. In this work, we limit ourselves to local collision operators. Finally, one should expect that the numerical accuracy and stability degrades to the lowest of the Ω^n and S_i^n used.

B. Common collision rules

In this section, the in literature commonly seen collision rules relevant for the applications presented in this paper are reiterated. This includes the following: BGK collision operator with the weakly compressible equilibrium distribution, fullway bounceback (BB), equilibrium scheme (ES), antibounceback (ABB), and Robin boundary condition (RBC).

1. Single relaxation time

The BGK collision operator models transport phenomena processes as a relaxation of f_i to the equilibrium distribution f_i^{eq} with a single characteristic time τ [38],

$$\Omega^{\text{BGK}}[f_i] = -\frac{1}{\tau}\big(f_i - f_i^{\text{eq}}\big). \tag{9}$$

Fluid flow is characterized through the transport of momentum, with the equilibrium distribution defined by the moments of f. Advection of scalars, e.g., concentration, requires the velocities to be imposed in the equilibrium distribution. The relaxation time τ is defined from the nondimensional kinematic viscosity $\nu = c_s^2(\tau - \Delta t/2)$ or diffusivity $D = c_s^2(\tau - \Delta t/2)$, respectively, where c_s is the lattice speed of sound.

In LBM, the transport phenomena properties are defined by the equilibrium function. Different f_i^{eq} are used to characterize e.g., weakly compressible, linear or incompressible transport (Chap. 4 in Ref. [2]). The weakly compressible

equilibrium function commonly used in the collision above is given as

$$f_i^{\mathrm{eq}}(\rho,\mathbf{u}) = w_i\rho\left(1+\frac{c_{i\alpha}u_\alpha}{c_s^2}+\frac{u_\alpha u_\beta\left(c_{i\alpha}c_{i\beta}-c_s^2\delta_{\alpha\beta}\right)}{2c_s^4}\right), \tag{10}$$

where $\{w_i\}$ is the lattice weight set, derived from the discretized Boltzmann distribution [2]. Here $\delta_{\alpha\beta}$ is the Kronecker delta. For clarity, the density and velocity used to compute f_i^{eq} can be denoted as ρ^{eq} and $\mathbf{u}^{\mathrm{eq}}$.

2. Fullway bounceback

The halfway BB condition used to implement static no-slip or adiabatic walls, i.e., zero velocity Dirichlet boundary condition, is given as [39,40]

$$f_{\bar{i}}(\boldsymbol{x},t+\Delta t) = f_i^\star(\boldsymbol{x},t), \tag{11}$$

where $f_i^\star(\boldsymbol{x},t)$ is the postcollision state. The notation $\bar{i}$ indicates the opposite direction of i, i.e., $\mathbf{c}_{\bar{i}} = -\mathbf{c}_i$. The $f_i^\star(\boldsymbol{x},t)$ depends on the preceding collision, e.g., for LBGK it is $f_i^\star(\boldsymbol{x},t) = f_i + \Omega^{\mathrm{BGK}}[f_i]\Delta t$.

Following Refs. [2,4], the solid boundary condition is expressed as a local collision rule, such that it is compatible with Eq. (3). The halfway BB boundary condition can be approximated as a collision rule within the wall

$$\Omega^{\mathrm{BB}}[f_i]\Delta t = -f_i + f_{\bar{i}} + 2w_i\rho_w\frac{c_{i\alpha}u_{w_\alpha}}{c_s^2}, \tag{12}$$

moving with velocity $\mathbf{u}_w$, where the subscript w is referring to the properties at the wall.

This is known as the fullway BB version and is simpler to implement in code. The unknown f_i are determined in the wall next to the interface and then streamed into the fluid domain in the next time step (Chap. 5 in Ref. [2]). This, however, introduces an time delay of one Δt.

With the same scheme, it is possible to approximate a mass or concentration density Neumann boundary condition to a velocity Dirichlet boundary condition for advection-diffusion processes [2,41]. The resulting approximated collision rule is

$$\Omega^{\mathrm{BB}}[f_i]\Delta t = -f_i + f_{\bar{i}} + 2w_i\frac{c_{i\alpha}q_{w_\alpha}}{c_s^2}, \tag{13}$$

where $\mathbf{q}_w$ is the applied flux of the Neumann boundary condition.

3. Fullway antibounceback

The ABB boundary condition [37,41–44] is a popular method to describe a density Dirichlet boundary condition in LBM. Similarly to the fullway BB, it can be expressed as a collision rule in the adjacent cell

$$\Omega^{\mathrm{ABB}}[f_i]\Delta t = -f_i - f_{\bar{i}} + 2w_i\rho_w\left(1+\frac{u_{w_\alpha}u_{w_\beta}\left(c_{i\alpha}c_{i\beta}-c_s^2\delta_{\alpha\beta}\right)}{2c_s^4}\right). \tag{14}$$

4. Equilibrium scheme

This simple scheme [45,46] is a method of describing both density and velocity by defining the populations directly by its equilibrium. Hence, its collision rule is given by

$$\Omega^{\mathrm{ES}}[f_i]\Delta t = -f_i + f_i^{\mathrm{eq}}. \tag{15}$$

Note that the ρ^{eq} and $\mathbf{u}^{\mathrm{eq}}$ are imposed and not necessarily that of the fluid. This collision rule can also be written in terms of the Ω^{ABB} Eq. (14) and Ω^{BB} Eq. (12). Expressing f_i^{eq} [cf. Eq. (10)] in terms of symmetric (+) and antisymmetric parts (–) in velocity space [41] gives

$$f_i^{\mathrm{eq}} = f_i^{\mathrm{eq}+} + f_i^{\mathrm{eq}-}, \quad \text{with} \quad f_i^{\mathrm{eq}\pm} = \frac{f_i^{\mathrm{eq}} \pm f_{\bar{i}}^{\mathrm{eq}}}{2}. \tag{16}$$

They have the properties that

$$f_{\bar{i}}^{\mathrm{eq}+} = f_i^{\mathrm{eq}+}, \quad \text{and} \quad f_{\bar{i}}^{\mathrm{eq}-} = -f_i^{\mathrm{eq}-}. \tag{17}$$

In this specific case, $f_i^{\mathrm{eq}+}$ contains the even-order velocity terms and $f_i^{\mathrm{eq}-}$ the odd-order velocity terms of f_i^{eq} [cf. Eq. (10)]. Then Ω^{ABB} and Ω^{BB} are given by

$$\Omega^{\mathrm{BB}}[f_i]\Delta t = -f_i + f_{\bar{i}} + 2f_i^{\mathrm{eq}-}, \tag{18}$$

$$\Omega^{\mathrm{ABB}}[f_i]\Delta t = -f_i - f_{\bar{i}} + 2f_i^{\mathrm{eq}+}. \tag{19}$$

From this follows that

$$\frac{\Omega^{\mathrm{ABB}}[f_i] + \Omega^{\mathrm{BB}}[f_i]}{2} = \Omega^{\mathrm{ES}}[f_i]. \tag{20}$$

This relation shows that the equilibrium scheme Ω^{ES} can be decomposed into Ω^{ABB} and Ω^{BB} with equal proportions—it is both a density and velocity Dirichlet boundary. Additionally, subtracting Ω^{BB} from Ω^{ABB}, and using Eq. (17), results in the following relation:

$$\frac{\Omega^{\mathrm{ABB}}[f_i] - \Omega^{\mathrm{BB}}[f_i]}{2} = \Omega^{\mathrm{ES}}[f_{\bar{i}}]. \tag{21}$$

5. Robin boundary condition

This boundary condition is a combination of both a density Dirichlet and Neumann boundary condition. It describes the mass flux for density fields, first-order reactions for concentration fields, or convection boundaries for temperature fields, with the relevant macroscopic equation

$$\mathbf{q}_w = -D\frac{\partial\rho}{\partial\mathbf{x}} = k_r\left(\rho_w^{\mathrm{eq}} - \rho\right). \tag{22}$$

Here k_r is the transfer coefficient and ρ_w^{eq} is the equilibrium at the wall. It models behavior between zero flux, $k_r = 0$, and infinitely fast, $k_r \to \infty$, transfer rate [33–36,47].

For a general local first-order equilibrium reaction without velocity [34–36], it was shown that a unified formulation can be derived [33]. Here we show the scheme found in literature, and its rewritten form as a collision rule

$$f_i^\star = \frac{2k_i}{1+k_i}w_i\rho_w^{\mathrm{eq}} + \frac{1-k_i}{1+k_i}f_{\bar{i}}, \tag{23}$$

$$\Omega^{\mathrm{RBC}}[f_i]\Delta t = -f_i + \frac{2k_i}{1+k_i}w_i\rho_w^{\mathrm{eq}} + \frac{1-k_i}{1+k_i}f_{\bar{i}}. \tag{24}$$

The $k_i = \gamma\, k_r\, (\mathbf{c}_i \cdot \mathbf{n})/c_s^2$ is the directional transfer rate, $\mathbf{n}$ is the wall normal pointing into the fluid, and $\gamma = \tau/(\tau - \Delta t/2)$ is a diffusion correction term. The different schemes in literature differ slightly in the definition of k_i.

C. Forcing in composite collisions

The force density in LBM is effectively a momentum source

$$\Delta(\rho\mathbf{u})^n = \boldsymbol{K}^n \Delta t. \tag{25}$$

There are two central questions for the inclusion of forces in the composite collision framework: (1) How are force densities decomposed and (2) how do forcing terms manifest for the composite collision components n.

The general answer to (1) is

$$\boldsymbol{K}^n = \eta^n \boldsymbol{K}. \tag{26}$$

A straightforward argumentation is that one actually applies an acceleration field $\mathbf{a}$, which all components experience equally $\mathbf{a}^n = \mathbf{a}$. Thus $\boldsymbol{K} = \rho\mathbf{a}$ and hence $\boldsymbol{K}^n = \rho^n\mathbf{a}$.

For question (2), it depends on the composite collision components n. Additionally, the forcing terms can manifest indirectly through the the equilibrium velocity $\mathbf{u}^{\mathrm{eq}n}$, or directly via S_i^n. Here we will discuss it first for the special case of velocity boundary conditions, at the hand of Ω^{BB}, and then for the general case, taking Ω^{BGK} as a final example.

The Ω^{BB} is a velocity Dirichlet boundary condition, where the velocity is prescribed. Thus the momentum source due to the force density [cf. Eq. (25)] is overwritten and resulting in $\mathbf{u}^{\mathrm{eq}\,\mathrm{BB}} = \mathbf{u}_w$ and $S_i^{\mathrm{BB}} = 0$. A different argumentation from microscopic perspective is that the BB populations "travel" $\Delta t/2$ with the accelerating field and $\Delta t/2$ against, thus canceling out the effect.

Continuing with the general case, forcing schemes in LBM can be differentiated in their source term S_i^n and how they modify the equilibrium velocity,

$$\mathbf{u}^{\mathrm{eq}n} = \frac{1}{\rho^n}\sum_i f_i^n \mathbf{c}_i + B\frac{\boldsymbol{K}^n \Delta t}{\rho^n}, \tag{27}$$

where B is a parameter depending on the forcing scheme. We will elucidate CCF properties by analyzing both, starting with the $\mathbf{u}^{\mathrm{eq}n}$.

In the absence of mass sources $\Delta\rho^n = 0$, the relation $\rho^n = \eta^n\rho$ holds and one can simplify Eq. (27) to

$$\mathbf{u}^{\mathrm{eq}n} = \frac{1}{\rho}\sum_i f_i \mathbf{c}_i + B\mathbf{a}^n \Delta t, \tag{28}$$

where $\mathbf{a}^n = \boldsymbol{K}^n/\rho^n$ is the acceleration experienced and $\mathbf{a}^n = \mathbf{a} = \boldsymbol{K}/\rho$. Immediately, we can see that the velocity is not dependent on the η^n.

With a lack of mass sources, the term S_i^n is solely a momentum source due to forces and $\sum_i S_i^n = 0$. Given Eqs. (26) and (25), the source term should be proportional to the composite fraction $S_i^n \propto \eta^n$ for $n \neq \mathrm{BB}$. A simple thought experiment to show that is as follows; let us assume the collision is momentum conserving $\sum_i \Omega^n[f_i^n]\mathbf{c}_i = 0$. That then leads to $\sum_i S_i^n \mathbf{c}_i = \boldsymbol{K}^n = \eta^n \boldsymbol{K}$. Therefore, $S_i^n \propto \eta^n$.

For a complete example, let us look at Ω^{BGK}. The resulting momentum with that new equilibrium velocity [cf. Eq. (28)] is

$$\begin{aligned}\sum_i \Omega^{\mathrm{BGK}}\big[f_i^{\mathrm{BKG}}\big]c_{i\alpha} &= -\frac{1}{\tau}\sum_i \big(f_i^{\mathrm{BGK}} - f_i^{\mathrm{eq}\,\mathrm{BGK}}\big)c_{i\alpha},\\ &= -\frac{\eta^{\mathrm{BGK}}}{\tau}\left(\sum_i (f_i c_{i\alpha}) - \rho u_\alpha^{\mathrm{eq}}\right),\\ &= \frac{\eta^{\mathrm{BGK}}\rho}{\tau} B a_\alpha \Delta t.\end{aligned} \tag{29}$$

Due to the second-order time discretization with forces, the BGK collision operator is not momentum conserving, and we have a momentum shift (Chap. 6 in Ref. [2]). This can be used directly, i.e., $B = \tau$, to immediately achieve the wanted force $\boldsymbol{K}^{\mathrm{BGK}} = \eta^{\mathrm{BGK}}\rho\mathbf{a}$.

Including the source term S_i^{BGK} to get the complete momentum source, we get

$$\begin{aligned}\sum_i \big(\Omega^{\mathrm{BGK}}\big[f_i^{\mathrm{BKG}}\big] + S_i^{\mathrm{BGK}}\big)c_{i\alpha} &= K_\alpha^{\mathrm{BGK}}\\ \frac{\eta^{\mathrm{BGK}}\rho}{\tau} B a_\alpha \Delta t + \sum_i S_i^{\mathrm{BGK}} c_{i\alpha} &= K_\alpha^{\mathrm{BGK}}\\ \sum_i S_i^{\mathrm{BGK}} c_{i\alpha} &= \left(1 - \frac{B\Delta t}{\tau}\right)K_\alpha^{\mathrm{BGK}}.\end{aligned} \tag{30}$$

The parameter B can be chosen, only impacting higher-order terms. Three options are usually taken: (1) $B = \tau$ will cancel out the explicit source term, which results in the Shan-Chen forcing method [48]; (2) $B = 0$ will remove the force modification from the equilibrium velocity, which is used by the exact difference method [49]; and (3) $B = 1/2$ will set the equilibrium velocity to the fluid velocity, which is used by two forcing schemes of Guo *et al.* [50] and He *et al.* [51]. Additionally, we have not defined S_i^n but found that $S_i^n \propto \eta^n$ and looked at the properties of the first two velocity moments. For the BGK, we can state that

$$S_i^{\mathrm{BGK}} = \left(1 - \frac{B\Delta t}{\tau}\right)\eta^{\mathrm{BGK}} K_i, \tag{31}$$

where K_i is any form of the discretized force $\boldsymbol{K}$, available in literature, see Chap. 6.4 in Ref. [2] for a summary. The second and above velocity moments of K_i depend on the f_i^{eq} chosen [52].

To conclude, forcing terms in CCF only need minor modifications. In general, the velocity is independent of the composite fraction and is equal for all component parts. The only location introducing the composite fraction is at the source term. These rules do not apply to collision steps which prescribed velocities, such as BB which is a velocity Dirichlet boundary conditions.

III. APPLICATION

In this section we will present several applications and combinations of the shown methods. First, the composite collision framework is applied to analyze a RBC Sec. III A, providing key insights and demonstrating a straightforward way to extend it. Afterwards, two new applications are

introduced, covering partially reactive walls Sec. III B and reactive membranes Sec. III C.

A. Analysis of advection-diffusion flux boundary conditions

In this section, we will show how CCF can be applied to rewrite existing collision steps. We show this procedure by analyzing a Robin-type boundary condition [cf. Eq. (24)]. The aim is to provide, on the one hand, better physical insight to the RBC in LBM and, on the other hand, show how rewriting can be advantageous for implementation of complex operators. In CCF the bulk is simulated with Ω^{BGK} and we only consider the boundaries here.

1. Physical insight

The RBC is a linear combination of the Dirichlet and Neumann boundary condition. From Sec. II B, the Dirichlet boundary condition set via Ω^{ABB} and the Neumann boundary condition can be approximated by Ω^{BB}.

The Ω^{RBC} [cf. Eq. (24)] recovers in its extremes of $k_i = 0$ and $k_i \to \infty$ the Ω^{BB} and Ω^{ABB} collision steps, respectively. Using those as the basis for a composite collision gives

$$\Omega^{\mathrm{RBC}}[f_i] = \sum_{n\in C} \Omega^n\left[f_i^n\right] = \Omega^{\mathrm{ABB}}\left[f_i^{\mathrm{ABB}}\right] + \Omega^{\mathrm{BB}}\left[f_i^{\mathrm{BB}}\right], \quad (32)$$

with the collision set $C = \{\mathrm{BB},\ \mathrm{ABB}\}$.

From the CCF the following relations hold, $\eta^{\mathrm{BB}} + \eta^{\mathrm{ABB}} = 1$ and $\rho_w^n = \eta^n \rho_w$. Hence, due to the linearity of the collision steps, one can factor out the η^n, and Eq. (32) becomes

$$\Omega^{\mathrm{RBC}}[f_i] = \eta^{\mathrm{ABB}}\Omega^{\mathrm{ABB}}[f_i] + \eta^{\mathrm{BB}}\Omega^{\mathrm{BB}}[f_i]. \quad (33)$$

Then using the decomposed ES formulations [cf. Eq. (20)], allows for combining Eqs. (33) and (20) and writing the composite RBC as

$$\Omega^{\mathrm{RBC}}[f_i] = 2\eta^{\mathrm{ABB}}\Omega^{\mathrm{ES}}[f_i] + (\eta^{\mathrm{BB}} - \eta^{\mathrm{ABB}})\Omega^{\mathrm{BB}}[f_i]. \quad (34)$$

To relate this composite collision formulation of the RBC with the one from literature [cf. Eq. (24)], it needs to be rewritten. Realizing that the two fractions in the scheme always add to 1, i.e., $(2k_i)/(1+k_i) + (1-k_i)/(1+k_i) = 1$, and for simplicity setting $\mathbf{c}_i \cdot \mathbf{n} = N$ to a constant, allows us to split the $-f_i$ term and express the literature RBC [cf. Eq. (24)] as a composite collision,

$$\Omega^{\mathrm{RBC}}[f_i] = \sum_{n\in C} \Omega^n\left[f_i^n\right] = \frac{2k_i}{1+k_i}\Omega^{\mathrm{ES}}[f_i] + \frac{1-k_i}{1+k_i}\Omega^{\mathrm{BB}}[f_i], \quad (35)$$

with the collision set $C = \{\mathrm{ES},\ \mathrm{BB}\}$.

Assuming that the RBC is the sole collision step allows us to compare Eqs. (35) and (34) for the computation of the composite fractions in Eq. (33). They are $\eta^{\mathrm{ABB}} = k_i/(1+k_i)$ and $\eta^{\mathrm{BB}} = 1/(1+k_i)$. Inserting the definition of k_i results in

$$\eta^{\mathrm{BB}} = \frac{1}{\tau N k_r/D + 1}. \quad (36)$$

A short discussion on the similarity of this BB composite fraction to the partial bounceback methods is given in Appendix B. When using the Ω^{RBC} as a fullway boundary collision, the wall normal can be reinserted $N = \mathbf{c}_i \cdot \mathbf{n}$.

Splitting the Ω^{RBC} in such a fashion allows for an easier analysis. Often the question is how much concentration, mass, or heat was added to the system. This is purely driven by the Ω^{ABB} only, and the Ω^{BB} does not contribute, i.e., $\Delta\rho^{\mathrm{BB}} = 0$ and $\Delta\rho = \Delta\rho^{\mathrm{ABB}}$.

2. Implementation

From a code implementation point of view, the RBC collision step [cf. Eq. (33)] requires adding a new collision function block. However, using CCF, it can be implemented in a way that reuses code. Starting at Eq. (33), we can rewrite Eq. (21) as $\Omega^{\mathrm{ABB}}[f_i] = \Omega^{\mathrm{BB}}[f_i] + 2\Omega^{\mathrm{ES}}[f_{\bar{i}}]$. Together, they form

$$\Omega^{\mathrm{RBC}}[f_i] = \eta^{\mathrm{ABB}}(\Omega^{\mathrm{BB}}[f_i] + 2\Omega^{\mathrm{ES}}[f_{\bar{i}}]) + \eta^{\mathrm{BB}}\Omega^{\mathrm{BB}}[f_i], \quad (37)$$

$$= \Omega^{\mathrm{BB}}[f_i] + 2\eta^{\mathrm{ABB}}\Omega^{\mathrm{ES}}[f_{\bar{i}}]. \quad (38)$$

In this rewritten form, we can see that the $\Omega^{\mathrm{RBC}}[f_i]$ can be expressed as a BB with a source. The source is dependent on $\Omega^{\mathrm{ES}}[f_{\bar{i}}] = f_{\bar{i}}^{\mathrm{eq}} - f_{\bar{i}}$, which is analogous to the $(\rho_w^{\mathrm{eq}} - \rho)$ in the first-order flux equation [cf. Eq. (22)]. It vanishes as the density difference approaches the equilibrium density.

To conclude this part, using the CCF, the RBC was broken down into simpler, better understood collision steps. This is useful for numerical analyses or Chapman-Enskog expansions, where instead of a new unfamiliar scheme, one has already published detailed derivations at hand [2,31,43,53].

Additionally, this analysis shows how (1) this RBC can be extended to include a wall velocity, by using the full BB and ABB equations Eqs. (12) and (14), (2) physically equivalent operators, such as NEBB or interpolated BB, can be used to generate new RBC collision steps; and (3) the RBC can be rewritten to a more code implementation friendly formulation, which should help in the speed of development.

B. Partial Robin boundary condition

In this example, the CCF is used to generate a new collision step—the partial RBC (PRBC). This collision can be used to model subgrid effects. The nucleation process is a good illustrative physical example. A nucleus's size is usually just a few nanometers, typically much smaller than the grid size of the simulation. Hence, a grid point is better simulated as a partially reactive wall, where the majority of the surface is nonreactive.

The PRBC effectively models a wall where only a section has some flux. This can be interpreted as an imposition of reactive and nonreactive surfaces. Reactive flows are used here for illustration purposes, but this is valid for mass or heat flows as well. The impact of this imposition is discussed near the end of this section.

The two collision rules being combined are Ω^{RBC}, discussed in Sec. III A, and Ω^{BB}. The resulting collision step reads

$$\Omega^{\mathrm{PRBC}}[f_i] = \sum_{n\in C} \Omega^n\left[f_i^n\right] = \Omega^{\mathrm{RBC}}\left[f_i^{\mathrm{RBC}}\right] + \Omega^{\mathrm{BB}}\left[f_i^{\mathrm{BB}}\right], \quad (39)$$

with the collision set $C = \{\mathrm{RBC},\ \mathrm{BB}\}$.

In the following, a pure diffusion problem is solved ($\mathbf{u} = 0$) which is used to compare a fully resolved alternating Ω^{RBC}

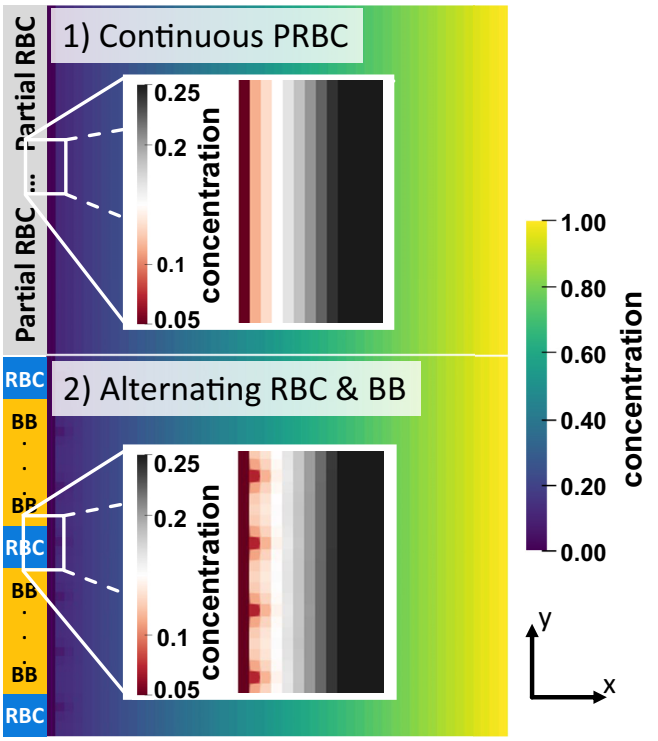

FIG. 1. Steady-state simulation results comparing the PRBC to the resolved BB-RBC setup. A spacing of $N_{\mathrm{BB}} = 5$ with a $\mathrm{Da} = 500$ is used. For the PRBC, the composite fraction used is $\eta^{\mathrm{RBC}} = 1/9$. The inset shows the behavior near the wall to highlight the effects in that region.

and Ω^{BB} boundary versus the proposed composite Ω^{PRBC}. A visual representation is shown for one particular case in Fig. 1, with a domain of 50×200. The Péclet number ($\mathrm{Pe} = LU/D$) is 1, and lattice velocity is $U = 0.02$. The reaction is defined via the Damköhler number ($\mathrm{Da} = k_r/U$) and k_r is varied. At the right boundary ($x = 50$), a density Dirichlet condition is set with $\rho = 1$, the domain in the y axis is periodic. In our nucleation example, ρ is representing concentration. The left boundary ($x = 0$), either consists of (1) the proposed continuous PRBC or (2) an alternating only reactive—only BB boundary condition.

The number of fully BB grid points between each RBC grid point is N_{BB} and will be used in the computation of η^{PRBC}. An example simulation comparing the two methods is given in Fig. 1, where the top half is the PRBC and the bottom half alternating fully reactive.

The comparison in Fig. 1 shows a spacing of $N_{\mathrm{BB}} = 5$ with a $\mathrm{Da} = 500$ and corresponding $\eta^{\mathrm{RBC}} = 1/9$ to match the alternating case. Other Damköhler numbers, spacing, and η^{RBC} values were also simulated and plotted in Fig. 2. For these simulations, the composite fraction is given by

$$\eta^{\mathrm{RBC}} = \frac{1}{AN_{\mathrm{BB}} + 1}. \tag{40}$$

Here A is a parameter to fit the composite to the resolved simulation result. Defining the composite fraction in this way is in line with approaches previously reported in the literature

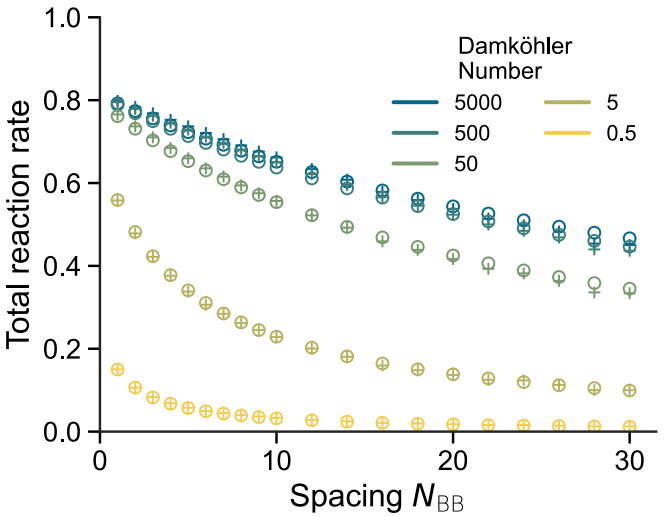

FIG. 2. Comparison of nondimensional reaction rates from boundary condition using the alternating (pluses) vs PRBC (circles). The spacing N_{BB} is varied between 1 and 30. The Damköhler numbers $\mathrm{Da} = \{0.5, 5, 50, 500, 5000\}$ were simulated, where the fitting parameter $A = \{1, 1, 1.3, 1.9, 2.0\}$ were used, respectively.

[cf. Eqs. (B1) and (36)]. Since only one reactive grid point is simulated $N_{\mathrm{RBC}} = 1$, the impact of multiple reactive grid points is not shown. However, logically, the relevant factor is $N_{\mathrm{BB}}/N_{\mathrm{RBC}}$. This is true especially for the reaction limited case ($\mathrm{PeDa} \ll 1$), where the exact positions of the reactive grid points are negligible.

Due the wall length being a fixed 200 grid points, certain N_{BB} spacings have the same number of fully reactive grid points. For example $N_{\mathrm{BB}} = \{22,\ 24\}$, and $N_{\mathrm{BB}} = \{28,\ 30\}$ have nine and seven reactive grid points, respectively. However, for the higher spacing of each of the two pairs, the distribution is slightly worse, hence decreasing the diffusion towards the reactive grid points and thus slightly decreasing total reactions, as can be seen in Fig. 2.

From Fig. 2, it is clear that the relation of Eq. (40) captures the behavior, as long as an appropriate value for A is used. A sensitivity analysis of A is given in Appendix C.

The parameter A is related to how reaction- or diffusion-limited the system is, with reaction limit $A = 1$ and diffusion limit $A \to A_{\mathrm{lim}}$. The A_{lim} is a constant related to the system geometry, which in our case is approximately 2. With some algebraic manipulation, Eq. (40) can be rewritten to

$$\eta^{\mathrm{RBC}} = \frac{1}{AN_{\mathrm{BB}}/N_{\mathrm{RBC}} + 1} = N_{\mathrm{RBC}}/(AN_{\mathrm{BB}} + N_{\mathrm{RBC}}). \tag{41}$$

When $A = 1$, Eq. (41) shows that η^{RBC} is the area fraction of the reactive substrate. The parameter A is then an area correction factor needed for the diffusion limited case. That is a consequence of the imposition. It assumes that the timescale within the grid point is very fast and thus negligible. That results in an effectively infinitely fast diffusion within the PRBC grid point. In case the setup is diffusion limited, the timescale becomes relevant, which can be represented as if there are effectively fewer N_{RBC} or more N_{BB}.

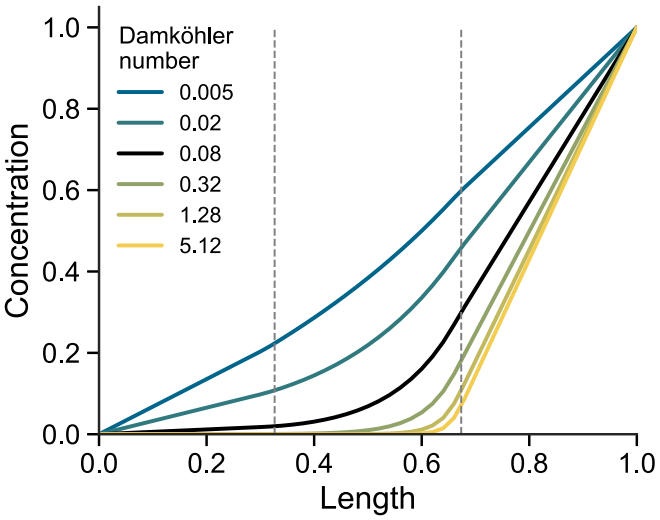

FIG. 3. Simulation results of semipermeable diffusion with a reactive membrane in between the dashed lines. The impact of variations of the reaction rate is shown. The black line is the common baseline. The composite fraction $\eta^{\mathrm{RBC}} = 0.1$.

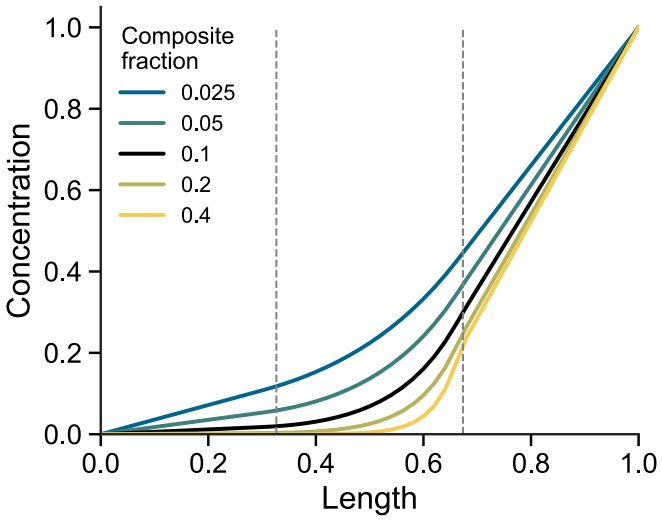

FIG. 4. Simulation results of semipermeable diffusion with a reactive membrane in between the dashed lines. The impact of variations of the composite fractions η^{RBC} are shown. The black line is the common baseline. The reaction rate is constant at $\mathrm{Da} = 0.08$.

C. Porous media with RBC surfaces

This showcase presents a diffusion case through a porous media with surfaces that are described by the RBC. The porous media is modeled via the partial bounceback [9]. Relevant examples are concentration diffusion through a reactive membrane or particulate mass flow through a dust filter. Macroscopically, the relevant processes are advection-diffusion (BGK) and Robin boundary condition (BB + ABB). In the CCF formulation, they results in a partial bounceback with fluxes (PBBF) collision step given as

$$\Omega^{\mathrm{PBBF}}[f_i] = \sum_{n\in C} \Omega^n\left[f_i^n\right] = \Omega^{\mathrm{RBC}}\left[f_i^{\mathrm{RBC}}\right] + \Omega^{\mathrm{BGK}}\left[f_i^{\mathrm{BGK}}\right], \tag{42}$$

with the collision set $C = \{\mathrm{RBC},\ \mathrm{BGK}\}$.

In the limit of no flux, $k_r = 0$ [cf. Eq. (36)], the RBC recovers the BB collision rule, thus the PBBF results in the known partial bounceback BGK-BB method [9]. For all transfer coefficients $k_r > 0$, it is a new collision step.

Intuitively, we can assume that a mixture of flow, wall and fluxes should result in some kind of semipermeable PBB with sources. Using the implementation friendly formulation of RBC [cf. Eq. (38)], we can indeed rewrite PBBF into

$$\Omega^{\mathrm{PBBF}}[f_i] = \Omega^{\mathrm{PBB}}[f_i] + 2\eta^{\mathrm{RBC}}\eta^{\mathrm{ABB}}\Omega^{\mathrm{ES}}[f_i]. \tag{43}$$

In this rewritten form, the PBBF clearly shows the advection-diffusion through porous media, with $\Omega^{\mathrm{PBB}}[f_i] = \Omega^{\mathrm{BGK}}[f_i^{\mathrm{BGK}}] + \Omega^{\mathrm{BB}}[f_i^{\mathrm{RBC}}]$, and has a source term of $+2\eta^{\mathrm{RBC}}\eta^{\mathrm{ABB}}\Omega^{\mathrm{ES}}[f_i]$. The $\Omega^{\mathrm{PBB}}[f_i]$ simulates diffusion with an effectively lower diffusivity due to tortuosity [9]. The η^{RBC} already contains τ-dependent corrective terms. Note the similarity to the macroscopic equation of diffusion and heterogeneous reactions in porous media [54].

This new collision step is showcased here as a reactive membrane in a quasi-1D reaction-diffusion problem. Simulations are performed on a 2D domain of size 10×50, periodic in the y axis, with two Dirichlet boundaries defining the concentration to $\rho = 0$ at $x = 0$ and $\rho = 1$ at $x = 50$. A semipermeable membrane is initialized from $x = 16$ to $x = 33$ with Ω^{PBBF}, Ω^{ABB} at the boundaries, and Ω^{BGK} elsewhere. The equilibrium concentration is $\rho^{\mathrm{eq}} = 0$, it is defined that $\mathbf{c}_i \cdot \mathbf{n} = 1$ for all i, the relaxation time is $\tau = 0.8$. A variation in the Damköhler number and composite fraction η^{RBC} is performed. The resulting concentration profile are shown in Figs. 3 and 4.

From the concentration profiles seen in Figs. 3 and 4, there are three distinct regions: the membrane indicated by the dashed box and the two freely diffusive regions to the left and right of the membrane. In the regions to the left and the right of the membrane, the concentration profile is linear, as one would expect for a constant diffusion coefficient. Inside the membrane, the concentration profile is increasing exponentially.

Both the Damköhler number and the composite fraction impact the reactivity of the membrane and, thus, the resulting concentration profile. The exponential is strongly determined by the composite fraction η^{RBC} (cf. Fig. 4). The Damköhler number has a larger impact on the concentration decrease than the composite fraction.

Since for advection-diffusion, the BB composite fraction is related to the tortuosity of the medium [9], changing this fraction allows studying the impact of a change in the tortuosity.

IV. CONCLUSION

We proposed a framework for composite collisions within the lattice Boltzmann method. This framework decomposes collision steps into component collision rules. For linear collision rules, this can be interpreted as splitting the total populations into component populations, applying a specific collision operator to each, before finally recombining them. This enables modeling of more complex physical phenomena through combination of various simple collision operators.

Special care has to be taken for the inclusion of forces in the scheme and we provide a general recipe for this aspect.

Benefits of the approach are demonstrated on several examples. It is shown how using this CCF approach may serve as a valuable analysis method. It is shown that the Robin boundary condition is a composition of bounceback and antibounceback collision rules. This insight allows an easier extension, to include moving walls or more accurate collision rules.

Additionally, the CCF was used to create two composite collision steps: the PRBC and PBBF. This demonstrates how the CCF can be used to synthesize new collision steps to capture nontrivial physical phenomena.

Several research avenues for the CCF remain open. One possibility is to account for intercollision interaction. Maybe it is possible to have microscopic velocity-dependent composite fractions, i.e., η_i^n. And, finally, investigating the CCF's applicability and limits for nonlocal collision rules. Overall, the framework provides a systematic approach to derive lattice Boltzmann methods for complex physical processes.

ACKNOWLEDGMENTS

The authors gratefully acknowledge financial support by the Federal Ministry of Education and Research (BMBF) within the project "SulForFlight" under the Grant No. 03XP0491A. M.L. and B.K. gratefully acknowledge financial support from the European Union's Horizon 2020 Research and Innovation Programme within the project "DEFACTO" under the Grant No. 875247. This work contributes to the research performed at CELEST (Center for Electrochemical Energy Storage Ulm-Karlsruhe).

J.W.: Conceptualization; Investigation; Methodology; Software; Visualization; Writing – original draft; B.K.: Conceptualization; Methodology; Validation; Writing – review & editing; M.P.L.: Conceptualization; Writing – review & editing; T.D.: Conceptualization; Funding acquisition; Project administration; Supervision; Writing – review & editing; A.L.: Funding acquisition; Supervision; Writing – review & editing;

DATA AVAILABILITY

The data are not publicly available. The data are available from the authors upon reasonable request.

APPENDIX A: COMPOSITE FRACTIONS FOR DARCY FLOW

In this section we will provide an example of how to relate the composite fraction η^n to the macroscopic variables. We will look at steady state flow through porous media, described by the macroscopic Darcy equation, and use the partial bounceback to model it. The η^n will always depend on the physics one wants to capture, and which dynamics and sources one chooses to apply. This example aims to provide guidance on how to apply this framework by using a well-studied problem. The partial bounceback method or gray LBM has been a popular approach to describe unresolved fluid flow in porous media. As presented here, it actually does not simulate porosity, only the drag effect of it. Here we will look at the composite collision of $n \in C = \{\mathrm{BGK},\ \mathrm{BB}\}$, which corresponds to the method of Ref. [9],

$$\Omega^{\mathrm{PBB}}[f_i] = \Omega^{\mathrm{BGK}}\big[f_i^{\mathrm{BGK}}\big] + \Omega^{\mathrm{BB}}\big[f_i^{\mathrm{BB}}\big]. \tag{A1}$$

The flow through the porous media is macroscopically described by the Darcy equation [55]

$$\mathbf{q} = -\frac{k}{\mu}\nabla p. \tag{A2}$$

The $\mathbf{q}$ is the volumetric flux, often called the superficial velocity, k is the permeability, and $\mu = \rho\nu$ is the dynamic viscosity. It is possible to rewrite this equation using the pressure-gradient force relation $\rho\mathbf{a} = \boldsymbol{K}^{\mathrm{Darcy}} = -\nabla p$, resulting in

$$\rho\mathbf{q} = \frac{k}{\nu}\boldsymbol{K}^{\mathrm{Darcy}}. \tag{A3}$$

Integrating over a discrete single time step Δt results in

$$\rho\mathbf{q}\Delta t = \frac{k}{\nu}\boldsymbol{K}^{\mathrm{Darcy}}\Delta t \quad\Longrightarrow\quad \frac{\nu\Delta t}{k} = \frac{\boldsymbol{K}^{\mathrm{Darcy}}\Delta t}{\rho\mathbf{q}}. \tag{A4}$$

The macroscopic superficial mass flux $\rho\mathbf{q}$ is equal to the CCF's total mass flux, i.e., $\rho\mathbf{u}$ [cf. Eq. (8)], computed as

$$\rho\mathbf{q} = \sum_i f_i c_{i\alpha} + \frac{1}{2}\Delta(\rho\mathbf{u}) = (1-\eta^{\mathrm{BB}})\sum_i f_i c_{i\alpha}. \tag{A5}$$

In the case of steady state there should be no change in momentum $\boldsymbol{K}^{\mathrm{Darcy}}\Delta t + \Delta(\rho\mathbf{u}) = 0$. The $\Delta(\rho\mathbf{u})$ is

$$\begin{aligned}
\Delta(\rho\mathbf{u}) &= \sum_i \big(\Omega^{\mathrm{PBB}}[f_i] + S_i^{\mathrm{PBB}}\big)c_{i\alpha},\\
&= \sum_i \Omega^{\mathrm{BGK}}\big[f_i^{\mathrm{BGK}}\big]c_{i\alpha} + \sum_i \Omega^{\mathrm{BB}}\big[f_i^{\mathrm{BB}}\big]c_{i\alpha},\\
&= \sum_i \big(-f_i^{\mathrm{BB}} + f_{\bar{i}}^{\mathrm{BB}}\big)c_{i\alpha}\\
&= -\sum_i f_i^{\mathrm{BB}} c_{i\alpha} - \sum_i f_{\bar{i}}^{\mathrm{BB}} c_{\bar{i}\alpha},\\
&= -2\eta^{\mathrm{BB}}\sum_i f_i c_{i\alpha}.
\end{aligned} \tag{A6}$$

Here we assume no additional forces, and thus $S_i^{\mathrm{PBB}} = 0$ and the BGK collision is momentum conserving, and for the BB we use the $\mathbf{c}_{\bar{i}} = -\mathbf{c}_i$ property. Inserting those definitions into Eq. (A4), and canceling out $\sum_i f_i\mathbf{c}_i$, results in

$$\frac{\nu\Delta t}{k} = \frac{2\eta^{\mathrm{BB}}}{1-\eta^{\mathrm{BB}}}. \tag{A7}$$

This relation is also found in the literature [6,9,56]. If the "half-source" correction is not considered, using the first-order LBM method, or using the fluid velocity instead of

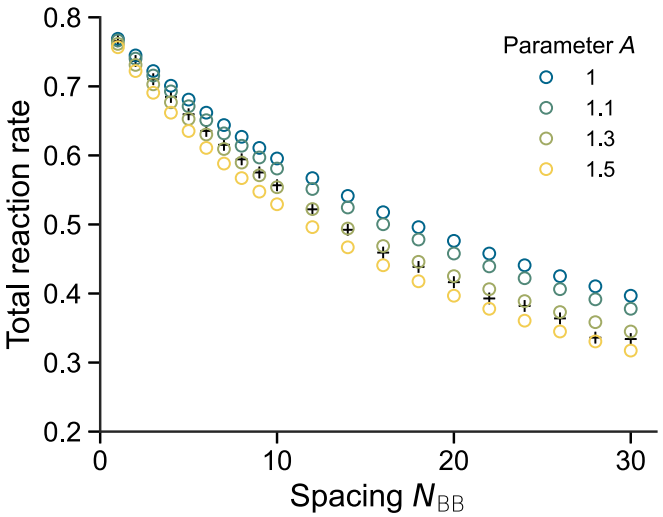

FIG. 5. Sensitivity of the fitting parameter A on simulated nondimensional reaction rated. The reaction rates of the boundary condition using the alternating BC (black pluses) vs PRBC (colored circles) are shown. The spacing N_{BB} is varied between 1 and 30. The Damköhler number $\mathrm{Da} = 50$ was simulated with fitting parameters $A = \{1,\ 1.1,\ 1.3,\ 1.5\}$.

superficial velocity, then the above relation will become

$$\frac{\nu \Delta t}{k} = 2\eta^{\mathrm{BB}}. \tag{A8}$$

That is found in Ref. [3] and taken over in Ref. [5]. Note that in literature, $\eta^{\mathrm{BB}} = n_s$, and is called solid fraction, which should be considered a misnomer. To capture the Darcy behavior, it does not matter from where the $\Delta(\rho \mathbf{u})$ originates from. Hence one can replace the $\Omega^{\mathrm{BB}}[f_i^{\mathrm{BB}}]$ with a pure source term S_i^{BB} of equivalent effect. Using a force to emulate boundaries is also known as the immersed boundary method. For porous media, that approach has already been shown to work, see, e.g., Ref. [57]. It can also be used to smooth the staircase interface, giving rise to diffuse interface methods, see, e.g., Refs. [4,31].

APPENDIX B: COMPARING RBC AND PBB COMPOSITE FRACTION

There are similarities between the forms of the η for different physical scenarios. For example, between RBC and PBB. Rewriting Eq. (A7) to solve for $\eta^{\mathrm{BB-PBB}}$, we find

$$\eta^{\mathrm{BB-PBB}} = \frac{1}{2k/(\nu \Delta t) + 1}. \tag{B1}$$

The bounceback composite fraction of RBC [cf. Eq. (36)] is reiterated here

$$\eta^{\mathrm{BB-RBC}} = \frac{1}{\tau N k_r / D + 1}.$$

For a fluid, the viscosity is the momentum diffusivity. Hence it makes sense that instead of viscosity the scalar diffusivity appears here. The transfer rate k_r is then analogous to the permeability k.

APPENDIX C: PRBC PARAMTER *A* SENSITIVITY

In the PRBC, the composite fraction η^{RBC} is dependent on a fitting parameter A [cf. Eq. (40)]. Here the sensitivity of this parameter is shown for one simulation. The $\mathrm{Da} = 50$ simulation is used, since it is neither diffusion nor reaction limited and thus should be most sensitive to variation of A. The results are shown in Fig. 5.

From Fig. 5, it can be concluded that the fitting parameter has the largest impact when the spacing is very large. For small spacing, the impact is negligible. Even for the worst case with large spacing, the simulation is more sensitive to a decrease in the reaction rate, than to a variation in the fitting parameter.

[1] R. Benzi, S. Succi, and M. Vergassola, The lattice Boltzmann equation: Theory and applications, Phys. Rep. **222**, 145 (1992).

[2] T. Krüger, H. Kusumaatmaja, A. Kuzmin, O. Shardt, G. Silva, and E. M. Viggen, *The Lattice Boltzmann Method: Principles and Practice*, Graduate Texts in Physics (Springer International Publishing, Cham, 2017).

[3] O. Dardis and J. McCloskey, Lattice Boltzmann scheme with real numbered solid density for the simulation of flow in porous media, Phys. Rev. E **57**, 4834 (1998).

[4] D. R. Noble and J. R. Torczynski, A lattice-Boltzmann method for partially saturated computational cells, Int. J. Mod. Phys. C **09**, 1189 (1998).

[5] D. Thorne and M. Sukop, Lattice Boltzmann model for the elder problem, in *Developments in Water Science* (Elsevier, 2004), Vol. 55, pp. 1549–1557.

[6] H. Yoshida and H. Hayashi, Transmission–reflection coefficient in the lattice boltzmann method, J. Stat. Phys. **155**, 277 (2014).

[7] J. Zhu and J. Ma, An improved gray lattice Boltzmann model for simulating fluid flow in multi-scale porous media, Adv. Water Resour. **56**, 61 (2013).

[8] J. Zhu and J. Ma, Extending a gray lattice Boltzmann model for simulating fluid flow in multi-scale porous media, Sci. Rep. **8**, 5826 (2018).

[9] S. D. Walsh, H. Burwinkle, and M. O. Saar, A new partial-bounceback lattice-Boltzmann method for fluid flow through heterogeneous media, Comput. Geosci. **35**, 1186 (2009).

[10] Y. Gao, W. Zhou, Z. Wen, R. Dou, and X. Liu, Meso-scale simulation of Li–O_2 battery discharge process by an improved lattice Boltzmann method, Electrochim. Acta **442**, 141880 (2023).

[11] G. G. Pereira, Grayscale lattice Boltzmann model for multiphase heterogeneous flow through porous media, Phys. Rev. E **93**, 063301 (2016).

[12] M. P. Lautenschlaeger, J. Weinmiller, B. Kellers, T. Danner, and A. Latz, Homogenized lattice Boltzmann model for simulating multi-phase flows in heterogeneous porous media, Adv. Water Resour. **170**, 104320 (2022).

[13] M. P. Lautenschlaeger, B. Prifling, B. Kellers, J. Weinmiller, T. Danner, V. Schmidt, and A. Latz, Understanding electrolyte filling of lithium-ion battery electrodes on the pore scale using the lattice Boltzmann method, Batteries Supercaps **5**, e202200090 (2022).

[14] G. Wang, U. D'Ortona, and P. Guichardon, Improved partially saturated method for the lattice Boltzmann pseudopotential multicomponent flows, Phys. Rev. E **107**, 035301 (2023).

[15] L. Vienne, S. Marie, and F. Grasso, Simulation of viscous fingering Instability by the lattice Boltzmann method, in *AIAA Aviation 2019 Forum* (American Institute of Aeronautics and Astronautics, Reston, VA, 2019).

[16] H. Yu, X. Chen, Z. Wang, D. Deep, E. Lima, Y. Zhao, and S. D. Teague, Mass-conserved volumetric lattice Boltzmann method for complex flows with willfully moving boundaries, Phys. Rev. E **89**, 063304 (2014).

[17] Z. Tian and J. Wang, Lattice Boltzmann simulation of CO_2 reactive transport in network fractured media: LBM CO_2 reactive transport, Water Resour. Res. **53**, 7366 (2017).

[18] Z. Sun, Y. Yin, Y. Wu, Z. Sun, L. Zhu, Y. Zhan, V. Niasar, and S. An, Morphological and hydrodynamic properties of hydrates during dissociation in sediment, Fuel **353**, 129032 (2023).

[19] P. Eibl, S. Rustige, C. Witz, and J. Khinast, LBM for two-phase (bio-)reactors, in *Advances in Chemical Engineering* (Elsevier, Amsterdam, 2020), Vol. 55, pp. 219–285.

[20] C. Zhan, X. Liu, Z. Chai, and B. Shi, A thermodynamically consistent and conservative diffuse-interface model for gas/liquid-liquid-solid flows, J. Comput. Phys. **532**, 113949 (2025).

[21] R. Petkantchin, A. Rousseau, O. Eker, K. Zouaoui Boudjeltia, F. Raynaud, B. Chopard, and the INSIST investigators, A simplified mesoscale 3D model for characterizing fibrinolysis under flow conditions, Sci. Rep. **13**, 13681 (2023).

[22] M. Gaedtke, S. Abishek, R. Mead-Hunter, A. J. C. King, B. J. Mullins, H. Nirschl, and M. J. Krause, Total enthalpy-based lattice Boltzmann simulations of melting in paraffin/metal foam composite phase change materials, Int. J. Heat Mass Transf. **155**, 119870 (2020).

[23] H. Li, H. Wei, T. P. Padera, J. W. Baish, and L. L. Munn, Computational simulations of the effects of gravity on lymphatic transport, PNAS Nexus **1**, pgac237 (2022).

[24] S. An, H. Erfani, H. Hellevang, and V. Niasar, Lattice-Boltzmann simulation of dissolution of carbonate rock during CO2-saturated brine injection, Chem. Eng. J. **408**, 127235 (2020).

[25] K. Han, Y. Feng, and D. Owen, Modelling of thermal contact resistance within the framework of the thermal lattice Boltzmann method, Int. J. Therm. Sci. **47**, 1276 (2008).

[26] X. Li, D. Gao, B. Hou, and X. Wang, An inserted layer LBM for thermal conduction with contact resistances, Chem. Eng. Sci. **233**, 116431 (2021).

[27] A. Mink, K. Schediwy, C. Posten, H. Nirschl, S. Simonis, and M. J. Krause, Comprehensive computational model for coupled fluid flow, mass transfer, and light supply in tubular photobioreactors equipped with glass sponges, Energies **15**, 7671 (2022).

[28] V. Aho, K. Mattila, T. Kühn, P. Kekäläinen, O. Pulkkinen, R. B. Minussi, M. Vihinen-Ranta, and J. Timonen, Diffusion through thin membranes: Modeling across scales, Phys. Rev. E **93**, 043309 (2016).

[29] W.-Z. Fang, H. Zhang, L. Chen, and W.-Q. Tao, Numerical predictions of thermal conductivities for the silica aerogel and its composites, Appl. Therm. Eng. **115**, 1277 (2017).

[30] C. Xie, J. Wang, D. Wang, N. Pan, and M. Wang, Lattice boltzmann modeling of thermal conduction in composites with thermal contact resistance, Commun. Comput. Phys. **17**, 1037 (2015).

[31] J. Liu, X. Liu, and Z. Chai, A diffuse-interface lattice Boltzmann method for thermal particulate flows with Dirichlet boundary conditions, Phys. Fluids **37**, 063303 (2025).

[32] J. Liu, C. Huang, Z. Chai, and B. Shi, A diffuse-interface lattice Boltzmann method for fluid–particle interaction problems, Comput. Fluids **233**, 105240 (2022).

[33] J. Weinmiller, M. P. Lautenschlaeger, B. Kellers, T. Danner, and A. Latz, General local reactive boundary condition for dissolution and precipitation using the lattice boltzmann method, Water Resour. Res. **60**, e2023WR034770 (2024).

[34] F. Verhaeghe, S. Arnout, B. Blanpain, and P. Wollants, Lattice-Boltzmann modeling of dissolution phenomena, Phys. Rev. E **73**, 036316 (2006).

[35] R. A. Patel, Lattice Boltzmann method based framework for simulating physico-chemical processes in heterogeneous porous media and its application to cement paste, Ph.D. thesis, Ghent University, 2016.

[36] L. Ju, C. Zhang, and Z. Guo, Local reactive boundary scheme for irregular geometries in lattice Boltzmann method, Int. J. Heat Mass Transf. **150**, 119314 (2020).

[37] T. Zhang, B. Shi, Z. Guo, Z. Chai, and J. Lu, General bounce-back scheme for concentration boundary condition in the lattice-Boltzmann method, Phys. Rev. E **85**, 016701 (2012).

[38] P. L. Bhatnagar, E. P. Gross, and M. Krook, A model for collision processes in gases. I. Small amplitude processes in charged and neutral one-component systems, Phys. Rev. **94**, 511 (1954).

[39] I. Ginzbourg and D. d'Humières, Local second-order boundary methods for lattice Boltzmann models, J. Stat. Phys. **84**, 927 (1996).

[40] A. J. C. Ladd, Numerical simulations of particulate suspensions via a discretized Boltzmann equation. Part 1. Theoretical foundation, J. Fluid Mech. **271**, 285 (1994).

[41] I. Ginzburg, Generic boundary conditions for lattice Boltzmann models and their application to advection and anisotropic dispersion equations, Adv. Water Resour. **28**, 1196 (2005).

[42] I. Ginzburg, F. Verhaeghe, and D. D'Humières, Two-relaxation-time lattice Boltzmann scheme: About parametrization, velocity, pressure and mixed boundary conditions, Commun. Comput. Phys. **3**, 427 (2008).

[43] I. Ginzburg, F. Verhaeghe, and D. D'Humières, Study of simple hydrodynamic solutions with the two-relaxation-times lattice Boltzmann scheme, Commun. Comput. Phys. **3**, 519 (2008).

[44] S. Izquierdo and N. Fueyo, Characteristic nonreflecting boundary conditions for open boundaries in lattice Boltzmann methods, Phys. Rev. E **78**, 046707 (2008).

[45] J. Latt, B. Chopard, O. Malaspinas, M. Deville, and A. Michler, Straight velocity boundaries in the lattice Boltzmann method, Phys. Rev. E **77**, 056703 (2008).

[46] X. He, Q. Zou, L.-S. Luo, and M. Dembo, Analytic solutions of simple flows and analysis of nonslip boundary conditions for the lattice Boltzmann BGK model, J. Stat. Phys. **87**, 115 (1997).

[47] J. Huang and W.-A. Yong, Boundary conditions of the lattice Boltzmann method for convection–diffusion equations, J. Comput. Phys. **300**, 70 (2015).

[48] X. Shan and H. Chen, Lattice Boltzmann model for simulating flows with multiple phases and components, Phys. Rev. E **47**, 1815 (1993).

[49] A. Kupershtokh, D. Medvedev, and D. Karpov, On equations of state in a lattice Boltzmann method, Comput. Math. Appl. **58**, 965 (2009).

[50] Z. Guo, C. Zheng, and B. Shi, Discrete lattice effects on the forcing term in the lattice Boltzmann method, Phys. Rev. E **65**, 046308 (2002).

[51] X. He, X. Shan, and G. D. Doolen, Discrete Boltzmann equation model for nonideal gases, Phys. Rev. E **57**, R13 (1998).

[52] The benefit of the second-order force moment has been cast in doubt recently [58].

[53] Q. Li and K. H. Luo, Effect of the forcing term in the pseudopotential lattice Boltzmann modeling of thermal flows, Phys. Rev. E **89**, 053022 (2014).

[54] F. J. Valdés-Parada, D. Lasseux, and S. Whitaker, Diffusion and heterogeneous reaction in porous media: The macroscale model revisited, Int. J. Chem. Reactor Eng. **15**, 20170151 (2017).

[55] S. Whitaker, Flow in porous media I: A theoretical derivation of Darcy's law, Transp. Porous Media **1**, 3 (1986).

[56] C. Chen, L. Li, R. Mei, and J. F. Klausner, Chapman–Enskog analyses on the gray lattice Boltzmann equation method for fluid flow in porous media, J. Stat. Phys. **171**, 493 (2018).

[57] I. Ginzburg, G. Silva, and L. Talon, Analysis and improvement of Brinkman lattice Boltzmann schemes: Bulk, boundary, interface. Similarity and distinctness with finite elements in heterogeneous porous media, Phys. Rev. E **91**, 023307 (2015).

[58] B. Postma and G. Silva, Force methods for the two-relaxation-times lattice Boltzmann, Phys. Rev. E **102**, 063307 (2020).